

Flow between two sites on a percolation cluster

José S. Andrade, Jr.,^{1,2} Sergey V. Buldyrev,¹ Nikolay V. Dokholyan,^{1,3} Shlomo Havlin,^{1,4} Peter R. King,⁵ Youngki Lee,^{1,*} Gerald Paul,¹ and H. Eugene Stanley¹

¹Center for Polymer Studies, Boston University, Boston, Massachusetts 02215

²Departamento de Física, Universidade Federal do Ceará, 60451-970 Fortaleza, Ceará, Brazil

³Department of Chemistry and Chemical Biology, Harvard University, 12 Oxford Street, Cambridge, Massachusetts 02138

⁴Minerva Center and Department of Physics, Bar-Ilan University, Ramat Gan, Israel

⁵Centre for Petroleum Studies, TH Huxley School, Imperial College, Prince Consort Road, London SW7 2BP, United Kingdom

(Received 21 April 2000; revised manuscript received 27 July 2000)

We study the flow of fluid in porous media in dimensions $d=2$ and 3. The medium is modeled by bond percolation on a lattice of L^d sites, while the flow front is modeled by tracer particles driven by a pressure difference between two fixed sites (“wells”) separated by Euclidean distance r . We investigate the distribution function of the shortest path connecting the two sites, and propose a scaling ansatz that accounts for the dependence of this distribution (i) on the size of the system L and (ii) on the bond occupancy probability p . We confirm by extensive simulations that the ansatz holds for $d=2$ and 3. Further, we study two dynamical quantities: (i) the minimal traveling time of a tracer particle between the wells when the total flux is constant and (ii) the minimal traveling time when the pressure difference is constant. A scaling ansatz for these dynamical quantities also includes the effect of finite system size L and off-critical bond occupation probability p . We find that the scaling form for the distribution functions for these dynamical quantities for $d=2$ and 3 is similar to that for the shortest path, but with different critical exponents. Our results include estimates for all parameters that characterize the scaling form for the shortest path and the minimal traveling time in two and three dimensions; these parameters are the fractal dimension, the power law exponent, and the constants and exponents that characterize the exponential cutoff functions.

PACS number(s): 47.55.Mh, 05.60.Cd, 64.60.Ak

I. INTRODUCTION

Percolation theory is a paradigmatic model for connectivity, originally introduced as a mathematical subject in the late 1950s. Thereafter, percolation theory has been found useful to characterize many disordered systems [1–13]. The aim of the present paper is to discuss the potential application of percolation theory as a convenient geometrical model for understanding numerous aspects of flow through porous rocks [14,15]. Special emphasis will be given to the study of oil displacement, i.e., how hydrocarbons propagate through geological formations between a pair of wells in the oil field. This work could also be applied to the breakthrough time for contamination of a water supply, or the time for released radioactive material to get from a leaking nuclear repository into the biosphere.

Oil fields are extremely complex, containing geological heterogeneities on a wide range of length scales from centimeters to kilometers [16]. These heterogeneities, caused by the sedimentary processes that deposited the rocks and the subsequent actions on the rock, such as fracturing by tectonic forces and mineral deposition from aquifer flow, have a significant impact on hydrocarbon recovery.

However, in many cases the rock can be separated into two types—high permeability (“good”) and low or zero permeability (“bad”)—and for all practical purposes we can assume that the flow takes place only in the good rock. The

spatial distribution of the rock types is often close to random, in which case the classical percolation problem is a good approximation. The place of the occupancy probability p is taken by the volume fraction of the good rock, called the net-to-gross ratio in the petroleum literature. Thus it is reasonable to model the oil reservoir as a percolation cluster.

The most common method of oil recovery is by displacement. Either water or a miscible gas (carbon dioxide or methane) is injected in a well (or wells) to displace the oil to other wells. Ultimately the injected fluid will break through into a production well where it must be separated from the oil, which is a very costly process. Once the injected fluid has broken through, the rate of oil production declines as more injected fluid is produced. For economic purposes it is important to know when the injected fluid will break through.

As a first-order approximation, we will model the flow between injector and producer wells using Darcy’s law (analogous to Ohm’s law in electrical current), which implies that the invading and displacing fluids are miscible and have equal viscosity. Preliminary studies of the breakthrough time for this model [15] limited the analysis to two dimensions and $p=p_c$, with no finite size effects. This paper extends that work to three dimensions and treats the effects of the off-critical bond occupation probability p and finite system size. The problem of the flow of two immiscible fluids of differing viscosities is analogous to diffusion-limited aggregation (DLA) in percolation and was studied in [17].

This paper also examines the correlation between overall system conductivity and breakthrough time, information highly relevant to the accurate prediction of oil well efficiency. We study this breakthrough time at two distinct boundary conditions: (i) at fixed total flux and (ii) at fixed pressure difference between the wells.

*Present address: School of Materials, Mechanical & Automation Engineering, Yanbian University of Science & Technology, Beishan St., Yanji City, Jilin Province, 133000, China.

In Sec. II, we summarize the scaling properties of a simple geometrical property—the shortest path—and test its scaling ansatz in the limit of $p \gg p_c$ and strong finite size effects. In Sec. III we apply the same ansatz to the minimal traveling time (the breakthrough time) at two distinct boundary conditions and determine its correlation with overall conductivity.

II. SHORTEST PATH

This section deals with the distribution of the shortest path between two sites on a percolation cluster. Because of the qualitative resemblance between the shortest path and the minimal traveling time of a tracer particle, the first step in understanding fluid transport between two sites in a percolation system is to characterize the geometrical properties of the shortest connecting path. For example, if we assume that the traveling time along a path is proportional to the path length (i.e., all velocities are equal), then we can obtain a rough estimate for the traveling time from purely geometrical arguments.

A. Basic distribution functions

The *shortest path* or *chemical distance* ℓ between two sites on a percolation cluster is defined as the shortest path connecting the two sites [18,19]. The typical value ℓ^* of the shortest path between two sites on a cluster scales with the geometrical distance r between these points as

$$\ell^* \sim r^{d_{\min}}, \quad (1)$$

where

$$d_{\min} = \begin{cases} 1.13 \pm 0.02 & (d=2) \\ 1.374 \pm 0.005 & (d=3) \end{cases} \quad (2)$$

is the fractal dimension of the shortest path [20,21].

Consider a hypercubic lattice of L^d sites. All information about the distribution of shortest paths is contained in the joint probability density function $P(r, \ell)$, i.e., the probability that two sites on the same spanning cluster are separated by geometrical distance r and chemical path ℓ . We sum over all chemical paths ℓ to calculate the probability distribution that the Euclidean distance between two sites is r ,

$$P(r) \equiv \int P(r, \ell) d\ell. \quad (3)$$

Similarly, we obtain the probability distribution that two sites are separated by the chemical distance ℓ by summing over all possible geometrical distances,

$$P(\ell) \equiv \int P(r, \ell) dr. \quad (4)$$

Given that the shortest distance between these sites is ℓ , the conditional probability that the geometrical distance between two sites is r is [3]

$$P(r|\ell) = \frac{P(r, \ell)}{P(\ell)}. \quad (5)$$

For isotropic media this function has been studied extensively and $P(r|\ell)$ is of the form [2,3,22–24]

$$P(r|\ell) \sim \frac{1}{\ell} \left(\frac{r}{\ell^{\tilde{\nu}}} \right)^{g_r} \exp \left[-a \left(\frac{r}{\ell^{\tilde{\nu}}} \right)^{\tilde{\delta}} \right], \quad (6)$$

where

$$\tilde{\delta} = \frac{1}{1 - \tilde{\nu}} = \frac{d_{\min}}{d_{\min} - 1} \quad (7)$$

and

$$\tilde{\nu} \equiv 1/d_{\min}. \quad (8)$$

For $d=2$, Ziff recently argued [25] that

$$g_r - 1 = 25/24 \quad (d=2). \quad (9)$$

The function of interest to us is the conditional probability for two sites to be separated by the shortest path ℓ , given that the geometrical distance between these sites is r :

$$P(\ell|r) = \frac{P(r, \ell)}{P(r)}. \quad (10)$$

From Eqs. (10) and (5), we see that $P(r|\ell)$ and $P(\ell|r)$ are related as

$$P(\ell|r) = P(r|\ell) \frac{P(\ell)}{P(r)}. \quad (11)$$

At the percolation threshold, it has been shown [14] that, in analogy with Eq. (6),

$$P(\ell|r) \sim \frac{1}{r^{d_{\min}}} \left(\frac{\ell}{r^{d_{\min}}} \right)^{-g_{\ell}} \exp \left[-a \left(\frac{\ell}{r^{d_{\min}}} \right)^{-\phi_{\ell}} \right], \quad (12)$$

where

$$g_{\ell} - 1 = \frac{(g_r - 1) + (2 - d_f)}{d_{\min}}, \quad (13)$$

$$\phi_{\ell} = \tilde{\delta} \tilde{\nu} = \tilde{\nu} / (1 - \tilde{\nu}) = \frac{1}{d_{\min} - 1}, \quad (14)$$

and

$$d_f = \begin{cases} 91/48 & (d=2) \\ 2.524 \pm 0.008 & (d=3) \end{cases} \quad (15)$$

is the fractal dimension of the incipient infinite cluster [1,3]. Substituting Eq. (9) into Eq. (13), we find for $d=2$

$$g_{\ell} = 2.01 \pm 0.02 \quad (d=2). \quad (16)$$

The probability distribution of more practical interest is $P'(\ell|r)$, defined in the same way as $P(\ell|r)$ but for any two randomly chosen points separated by geometrical distance r and on the same cluster, but not necessarily on the incipient infinite cluster [14]. $P'(\ell|r)$ has the same scaling form as in Eq. (12), but with g_{ℓ} replaced by [14]

$$g'_{\ell} = g_{\ell} + \frac{d-d_f}{d_{\min}}. \quad (17)$$

B. Scaling ansatz for shortest path

The complete scaling form of $P'(\ell|r)$, which accounts also for finite size effects and off-critical behavior, has been studied for $d=2$ and reported in [14]. Specifically, the following ansatz has been proposed [14]:

$$P'(\ell|r) \sim \frac{1}{r^{d_{\min}}} \left(\frac{\ell}{r^{d_{\min}}} \right)^{-g'_{\ell}} f_1 \left(\frac{\ell}{r^{d_{\min}}} \right) f_2 \left(\frac{\ell}{L^{d_{\min}}} \right) f_3 \left(\frac{\ell}{\xi^{d_{\min}}} \right), \quad (18)$$

where $\xi \sim |p-p_c|^{-\nu}$ is the pair connectedness length, and the scaling functions have the forms

$$f_1(x) \equiv \exp(-ax^{-\phi}), \quad (19)$$

$$f_2(x) \equiv \exp(-bx^{\psi}), \quad (20)$$

and

$$f_3(x) \equiv \exp(-cx). \quad (21)$$

The function f_1 accounts for the lower cutoff due to the constraint $\ell > r$, while f_2 and f_3 account for the upper cutoffs due to the finite size effect and the finite correlation length, respectively. Either f_2 or f_3 becomes irrelevant, depending on the magnitudes of L and ξ : for $L < \xi$, f_2 dominates the upper cutoff, otherwise f_3 dominates. We assume that the finite size effect and the effect of the concentration of the occupied sites are independent of each other, so that Eq. (18) can be represented as a product of the terms that are responsible for the finite size effect (f_2) and the effect of the concentration (f_3). Simulations for $d=2$ have been performed in [14] and support this assumption.

C. Behavior at criticality

Here we extend the study of $P'(\ell|r)$ to $d=3$. We numerically test the scaling conjecture (18) exactly at the percolation threshold $p=p_c$ —in which case $\xi=\infty$ so $f_3=f(0)=1$. We build clusters using the Leath algorithm [18,19,26]. Since the Leath algorithm corresponds to the process of selecting a random point on the lattice, the probability $P'(\ell|r)$ is equal to the probability that a pair of randomly selected points has chemical distance ℓ and geometrical distance r , given that they belong to the same cluster, a cluster that is not necessarily the infinite cluster. Hence Eq. (18) reduces to

$$P'(\ell|r) \sim \frac{1}{r^{d_{\min}}} \left(\frac{\ell}{r^{d_{\min}}} \right)^{-g'_{\ell}} f_1 \left(\frac{\ell}{r^{d_{\min}}} \right) f_2 \left(\frac{\ell}{L^{d_{\min}}} \right) \quad (p=p_c). \quad (22)$$

Figure 1(a) shows that, in the range $r^{d_{\min}} < \ell < L^{d_{\min}}$, $P'(\ell|r)$ has power law behavior with slope

$$g'_{\ell} = 2.3 \pm 0.1 \quad (d=3) \quad (23)$$

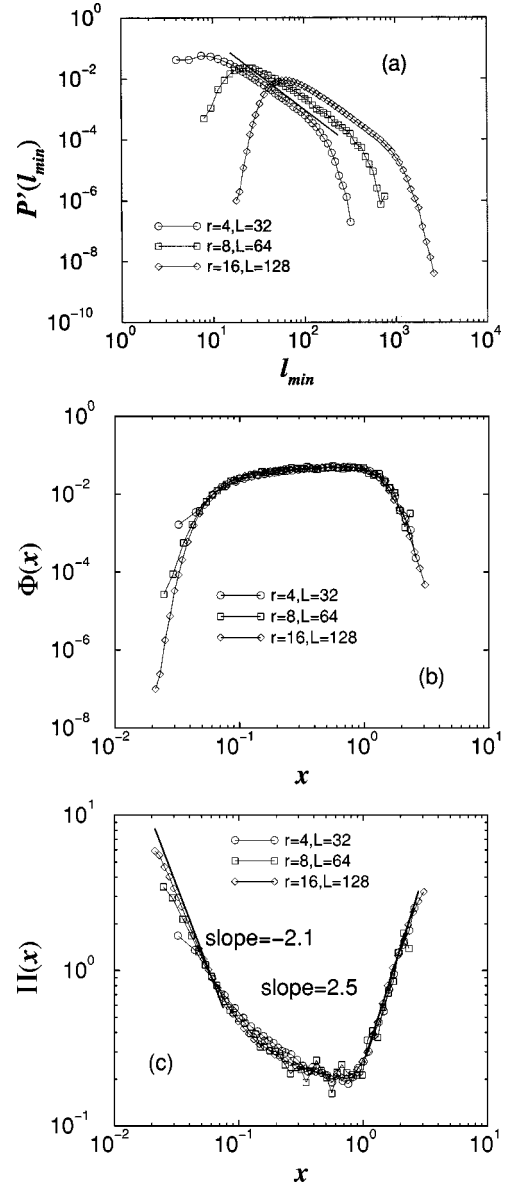


FIG. 1. For $d=3$, (a) log-log plot of $P'(\ell|r)$ at criticality ($p=p_c \approx 0.2488$) and for different sets of parameters: $(r,L) = (2,32), (4,64), (8,128)$. The straight line regime has slope $g'_{\ell} = 2.3$. (b) Log-log plot of rescaled probability $\Phi(x) \equiv P'(\ell|r) x^{g'_{\ell}} r^{d_{\min}}$ against rescaled length $x \equiv \ell/r^{d_{\min}}$ using the values $g'_{\ell} = 2.3$ and $d_{\min} = 1.39$. The curves are flat in the center because $f_2(x)$ is a stretched exponential [see Eq. (25)]. (c) Log-log plot of transformed probability $\Pi(x) = \log_{10}[A/\Phi(x)]$ versus $x = \ell/r^{d_{\min}}$. The slopes of the solid lines give the power of the stretched exponential function f_1 and f_2 in Eq. (25). Using the parameter $A = 0.08$, the slopes give $\phi \approx 2.1$ for the lower cutoff and $\psi \approx 2.5$ for the upper cutoff.

and rapidly vanishes for $\ell < r^{d_{\min}}$ and for $\ell > L^{d_{\min}}$. To determine the functions f_1 and f_2 , we compute the rescaled probability distribution

$$\Phi \left(\frac{\ell}{r^{d_{\min}}} \right) \equiv P'(\ell|r) \ell^{g'_{\ell}} r^{-d_{\min}(g'_{\ell}-1)}, \quad (24)$$

and plot it against the scaling variable $x \equiv \ell/r^{d_{\min}}$ [see Fig. 1(b)] using the value $d_{\min} = 1.374$. According to Eq. (22)

$$\Phi(x) = Af_1(x)f_2\left[x\left(\frac{r}{L}\right)^{d_{\min}}\right]. \quad (25)$$

Therefore, $\Phi(x)$ should depend only on x and the ratio r/L . Indeed, Fig. 1(b) shows excellent data collapse for $L/r=8$, with sharp cutoffs governed for $x<1$ by $f_1(x)$ and for $x>(L/r)^{d_{\min}}$ by $f_2[x(r/L)^{d_{\min}}]$.

In order to test the assumption that the functions f_1 and f_2 are stretched exponentials with exponents ϕ_ℓ and ψ_ℓ , we plot

$$\Pi(x) \equiv \log_{10}[A/\Phi(x)] \quad (26)$$

versus x in double logarithmic scale for various values of normalization constant A [see Fig. 1(c)]. If the stretched exponential conjecture is correct, $\Pi(x)$ should have two straight line asymptotes for $\log_{10} x \rightarrow +\infty$ with the slope ψ_ℓ and for $\log_{10} x \rightarrow -\infty$ with the slope $-\phi_\ell$. We find that the slopes ϕ_ℓ and ψ_ℓ of the straight line fits depend weakly on the value of A . Using $A=0.08$, we obtain the longest regimes of straight line behavior. For this value of A , we find $\phi_\ell \approx 2.1$ and $\psi_\ell \approx 2.5$. Equation (14) yields a predicted value of $\phi_\ell = 2.67$ in agreement with our simulation result.

D. Off-critical behavior

For $p \neq p_c$, we identify three regimes determined by the value of the connectedness length ξ in relation to the values of r and L .

(i) $\xi > L > r$. In this regime, the fact that $p \neq p_c$ cannot be detected because the connectedness length is larger than the other relevant variables.

(ii) $L > \xi > r$. In this case, the upper cutoff of the distribution Eq. (18) is governed by f_3 and the functional form of the rescaled probability Φ is given by

$$\Phi(\ell/r^{d_{\min}}) \sim f_1\left(\frac{\ell}{r^{d_{\min}}}\right)f_3\left(\frac{\ell}{\xi^{d_{\min}}}\right). \quad (27)$$

For large ℓ , we suggest an exponential decay [27] of Φ ,

$$\Phi(\ell/r^{d_{\min}}) \sim \exp\left(-c\frac{\ell}{\xi^{d_{\min}}}\right). \quad (28)$$

Indeed, for $p < p_c$, semilogarithmic plots of $\log\Phi(\ell/r^{d_{\min}})$ versus ℓ shown in Fig. 2(a) can be approximated by straight lines with slopes that approach zero as $p \rightarrow p_c$. According to Eq. (28), these slopes $k(p)$ should be proportional to $\xi^{-d_{\min}} \sim |p-p_c|^{d_{\min} \nu} \approx |p-p_c|^{1.19}$. Figure 2(b) shows a double logarithmic plot of $|k(p)|$ versus $|p-p_c|$ for $p < p_c$. This curve can be well approximated by a straight line with slope 1.22 in good agreement with the scaling conjecture (22). For $p > p_c$ a similar analysis should hold. However, limitations on the size of the system we can simulate make the analysis problematic. Figure 2(c) shows $P'(\ell)$ for various values of $p > p_c$. Note that it is only for values of $p \geq p_c + 0.03$ that the distributions ‘‘cut off’’ at smaller ℓ than the distribution for $p = p_c$. Thus it is only for values of $p - p_c \geq 0.03$ that the large ℓ behavior of Eq. (18) is determined by the fact that the system is not at criticality (i.e., by f_3) as opposed to being determined by the finite size of the system (i.e., by f_2).

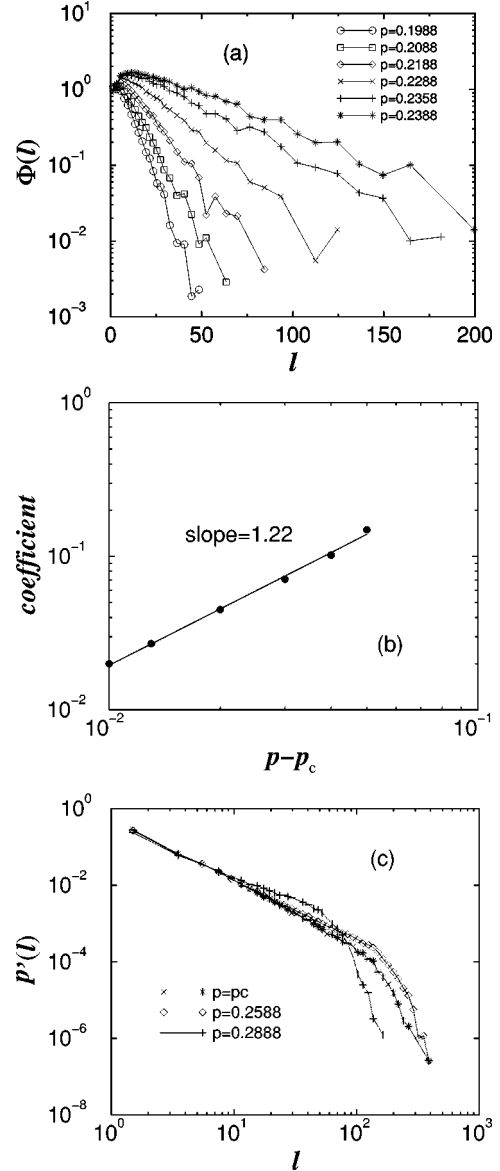


FIG. 2. For $d=3$, (a) semilogarithmic plot of transformed probability $\Phi(\ell)$ [see Eq. (25)] versus ℓ shows pure exponential behavior of f_3 . (b) The slope of the log-log plot of the coefficient in exponential function f_3 as a function of $|p-p_c|$ gives the value $\nu d_{\min} \approx 1.22$ for $p < p_c$. (c) $P'(\ell)$ for $p > p_c$. Note that it is only for $p \geq 0.2788$ that the large ℓ behavior is determined by the fact that the system is not at criticality.

Below $p = p_c + 0.03$, ξ is still greater than L . On the other hand, if p is not close to p_c , the scaling form is not expected to hold. Thus, the results are inconclusive based on the sizes of the systems we can generate—we cannot determine the parameters that govern the large ℓ behavior of Eq. (18) above p_c .

(iii) $L > r > \xi$. When the connectedness length ξ is smaller than the distance r between the wells, the system can be considered homogeneous [1,3,5]. This can be seen in Fig. 3(a) in which we plot $P(\ell/r)$ for various values of r at $p = 0.7$ for two-dimensional site percolation ($p_c = 0.593$). As r increases from below to above the connectedness length, the form of the distribution changes from the power law distribution of Eq. (18) to a Gaussian distribution with a pro-

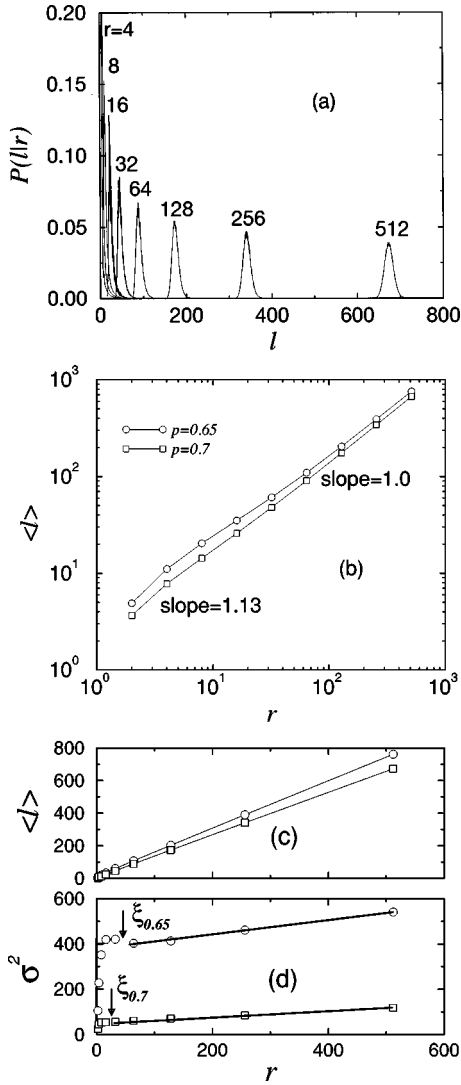


FIG. 3. For $d=2$, (a) distributions of $P(\ell|r)$ for $r=4,8,16,32,64,128,256,512$ and for $p=0.7$. To reduce the lattice effects, data are obtained for the pairs of wells on the x axis. [Note that for this case, where $r>\xi$, the distributions $P'(\ell|r)$ and $P(\ell|r)$ are essentially the same since all the clusters span the lattice.] The distributions converge for large r to a Gaussian with mean $\langle\ell\rangle$ shown in parts (b),(c) and variance $\sigma^2=\langle\ell^2\rangle-\langle\ell\rangle^2$ shown in part (d) as functions of r for $p=0.65$ (\circ) and $p=0.7$ (\square). (b) Log-log plot of $\langle\ell\rangle$ versus r . Note the crossover from power law behavior with exponent $d_{\min}=1.13$ to linear behavior with exponent 1.0. (c) Same as (b) on linear scale. The slopes of the linear fits $k(p)$ are 1.45 for $p=0.65$ and 1.30 for $p=0.7$. This yields $k(p)\sim(p-p_c)^{-0.17}$ in good agreement with equation Eq. (30). (d) The dependence of σ^2 versus r . According to Eq. (29), the dependence becomes linear only for $r>\xi\sim(p-p_c)^{-\nu}$, indicated on the graph. The slopes of linear fits $k(p)$ are 0.33 for $p=0.65$ and 0.12 for $p=0.7$. This gives $k(p)\sim(p-p_c)^{-1.6}$ in good agreement with Eq. (31).

nounced peak, a characteristic of homogeneous systems. Furthermore, as shown in Fig. 3(b), the fractal dimension of the shortest length crosses over from $d_{\min}=1.13$ to $d_{\min}=1.0$, characteristic of a homogeneous system [29,28]. The convergence to a Gaussian can be expected due to the following considerations. The minimal path connecting the wells separated by distance r passes through r/ξ independent blobs.

For each of these blobs, the probability distribution for the shortest path across the blob ℓ_b is still given by Eq. (18), but with r and L replaced by ξ and ℓ replaced by ℓ_b . This distribution is characterized by $\langle\ell_b\rangle\sim\xi^{d_{\min}}$ and variance $\sigma_b^2\equiv\langle\ell_b^2\rangle-\langle\ell_b\rangle^2\sim\xi^{2d_{\min}}$. The total minimal path is the sum of $n=r/\xi$ independent variables ℓ_b ; hence it converges to a Gaussian with

$$\langle\ell\rangle\sim r\xi^{d_{\min}-1} \quad \text{and} \quad \sigma^2\sim r\xi^{2d_{\min}-1}. \quad (29)$$

Thus the slope of the graph, $k(p)$, of $\langle\ell\rangle$ vs r in Fig. 3(c) should decay as

$$k(p)\sim|p-p_c|^{-\nu(d_{\min}-1)}=|p-p_c|^{-0.17} \quad (30)$$

and the slope of σ^2 versus r should decay as

$$|p-p_c|^{-\nu(2d_{\min}-1)}=|p-p_c|^{-1.7}. \quad (31)$$

Indeed [see Fig. 3(d)], we see that the slope of σ^2 versus r decays with p more strongly than that of $\langle\ell\rangle$ versus r . The numerical values of slopes from Figs. 3(c) and 3(d) are in good agreement with the theoretical predictions Eqs. (30) and (31). For $d=3$ we expect similar behavior.

III. MINIMAL TRAVELING TIME AND FASTEST PATH

We turn next to dynamics, the study of flow on percolation clusters, which has close ties to such applications as hydrocarbon recovery and ground-water pollution [3,30–33]. In this section, we discuss the properties of the flow on $d=2$ and $d=3$ bond percolation clusters. Specifically, we investigate the scaling properties of the distributions of *minimal traveling time* and the *length of the path corresponding to the minimal traveling time* (fastest path) of the tracer particles. Some of the results in $d=2$ were reported previously [15]. Here we extend the work to $d=3$, and study the effects of finite system size and off-criticality for $d=2$ and $d=3$.

A. The model

We study incompressible flow between two sites A and B separated by Euclidean distance r . To model the flow front, we use passive tracers—particles that are not absorbed by the surroundings, and move only by convection, ignoring molecular diffusion (which is slow on the time scales of interest). The convection is governed by the flow field due to the pressure difference between sites connected by the bonds. We simulate the flow of a tracer particle starting from the injection point A traveling through the medium along a path connected to the recovery point B . The dynamics of flow at a macroscopic level on the percolation cluster is determined by the local flow (local currents) on the individual bonds in the backbone of the cluster. The velocity of a tracer at each bond is determined by the pressure difference across that bond (Darcy's law [34]):

$$v_{ij}=T(P_j-P_i), \quad (32)$$

where P_i and P_j are the values of pressure at sites i and j . The coefficient T , which is a function of permeability k , viscosity η , and the length of a bond L_b [$T=k/(\eta L_b)$], is set to 1. We normalize the velocities, assuming that the total flow J

between A and B is fixed, independent of the distance between A and B , and the realization of the porous media. This more closely resembles oil recovery processes where constant flow, as opposed to constant pressure, is maintained.

We obtain the pressure difference across each bond by solving Kirchhoff's law

$$\sum_j v_{ij} = 0, \quad (33)$$

for each node i in the cluster where the summation is over all bonds connected to that node. We define the *traveling time* \tilde{t} of a path \mathcal{C} as the sum of the tracer's traveling times t_{ij} at each bond (ij) joining sites i and j which are on the path,

$$\tilde{t} = \sum_{(ij) \in \mathcal{C}} t_{ij}. \quad (34)$$

The *traveling length* $\tilde{\mathcal{L}}$, in turn, is the number of bonds present in path \mathcal{C} . Among the ensemble of all paths $\{\mathcal{C}\}$, we select the path \mathcal{C}^* that has the *minimal traveling time* t_{\min} ,

$$t_{\min}(\mathcal{C}^*) = \min_{\{\mathcal{C}\}} \tilde{t}(\mathcal{C}) \quad (35)$$

and we define the *length* of the fastest path ℓ_{\min} , corresponding to the minimal traveling time, as the number of bonds present in path \mathcal{C}^* . The first quantity t_{\min} is the breakthrough time of the gas/liquid that displaces the oil during recovery and has fundamental importance to the oil industry. The quantity \tilde{t} determines postbreakthrough behavior. We also define the exponents d_x , where x denotes ℓ_{\min} , t_{\min} , $\tilde{\mathcal{L}}$, or \tilde{t} by

$$x^* \sim r^{d_x}, \quad (36)$$

and where x^* is the characteristic (most probable) length or time of the corresponding distribution.

Using a ‘‘burning’’ algorithm [37], we then find the minimal time and the fastest path for the particle to travel between points A and B . At $t = t_{\min}$, the tracer particles spread over $t = Jt_{\min}$ bonds. These bonds constitute a subset of the backbone with fractal dimension d_{tm} , which is larger than the fractal dimension of the minimal path but smaller than the fractal dimension of the entire backbone d_B . Hence

$$d_{\min} < d_{\text{tm}} < d_B. \quad (37)$$

B. Minimal traveling time

We first study the minimal traveling time for $d = 2$. In Fig. 4, a scatter plot of the minimal traveling time versus shortest path, we see that the minimal times are strongly correlated with the shortest paths in the realizations simulated, $t_{\min} \sim \ell^z$, where $z \approx 1.17$. Since ℓ scales as $r^{d_{\min}}$ we propose that t_{\min} scales as $r^{d_{\text{tm}}}$ with $d_{\text{tm}} = zd_{\min} = 1.33$. This suggests that the same scaling form that applies to the distribution of shortest paths can also be applied to the distribution of minimal times, but with different exponents and amplitudes. Thus, we expect an ansatz similar to Eq. (18) to hold:

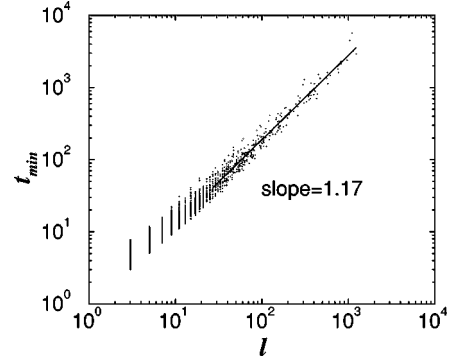


FIG. 4. For $d = 2$, scatter plot of the minimal traveling time t_{\min} versus shortest path ℓ for a fixed well separation $r = 1$. Note the strong correlation between t_{\min} and ℓ . The slope of the tail of the scatter plot is 1.17, yielding a values of $d_{\text{tm}} = 1.17$ and $d_{\min} = 1.32$, consistent with our result in Table I below.

$$P'(t_{\min}|r) \sim \frac{1}{r^{d_{\text{tm}}}} \left(\frac{t_{\min}}{r^{d_{\text{tm}}}} \right)^{-g'_{\text{tm}}} f_1 \left(\frac{t_{\min}}{r^{d_{\text{tm}}}} \right) f_2 \left(\frac{t_{\min}}{L^{d_{\text{tm}}}} \right) f_3 \left(\frac{t_{\min}}{\xi^{d_{\text{tm}}}} \right), \quad (38)$$

where the scaling functions are $f_1(x) = \exp(-a_{\text{tm}}x^{-\phi_{\text{tm}}})$, $f_2(x) = \exp(-b_{\text{tm}}x^{\psi_{\text{tm}}})$, and $f_3(x) = \exp(-c_{\text{tm}}x^{\pi_{\text{tm}}})$. Here ξ is a characteristic length of the pair connectedness function and has a power law dependence on the occupancy probability p as

$$\xi \sim |p - p_c|^{-\nu}. \quad (39)$$

The first function f_1 accounts for the lower cutoff due to the constraint $\ell > r$, while f_2 and f_3 account for the upper cutoffs due to the finite size effect and the finite connectedness length, respectively. Either f_2 and f_3 becomes irrelevant, depending on which of the two values L or ξ is greater. For $L < \xi$, f_2 dominates the upper cutoff, otherwise f_3 dominates. Since we have assumed independence of the finite size effect and off-criticality effect, Eq. (38) can be represented as a product of the terms that are responsible for the finite size effect (f_2) and the effect of the concentration (f_3).

We sample over 10^6 different realizations with the two sites A and B fixed. For each realization, we calculate exactly the minimal traveling time and the path that corresponds to the minimal traveling time to obtain $P(t_{\min})$ and $P(\ell_{\min})$.

1. Behavior at criticality

We first test numerically the scaling conjecture Eq. (38) at the percolation threshold $p = p_c$. In this case, $\xi = \infty$ and f_3 is a constant. Hence Eq. (38) reduces to

$$P'(t_{\min}|r) \sim \frac{1}{r^{d_{\text{tm}}}} \left(\frac{t_{\min}}{r^{d_{\text{tm}}}} \right)^{-g'_{\text{tm}}} f_1 \left(\frac{t_{\min}}{r^{d_{\text{tm}}}} \right) f_2 \left(\frac{t_{\min}}{L^{d_{\text{tm}}}} \right) \quad (p = p_c). \quad (40)$$

Figure 5(a) shows that $P'(t_{\min}|r)$ has a power law regime with slope

$$g'_{\text{tm}} = 2.0 \pm 0.1. \quad (41)$$

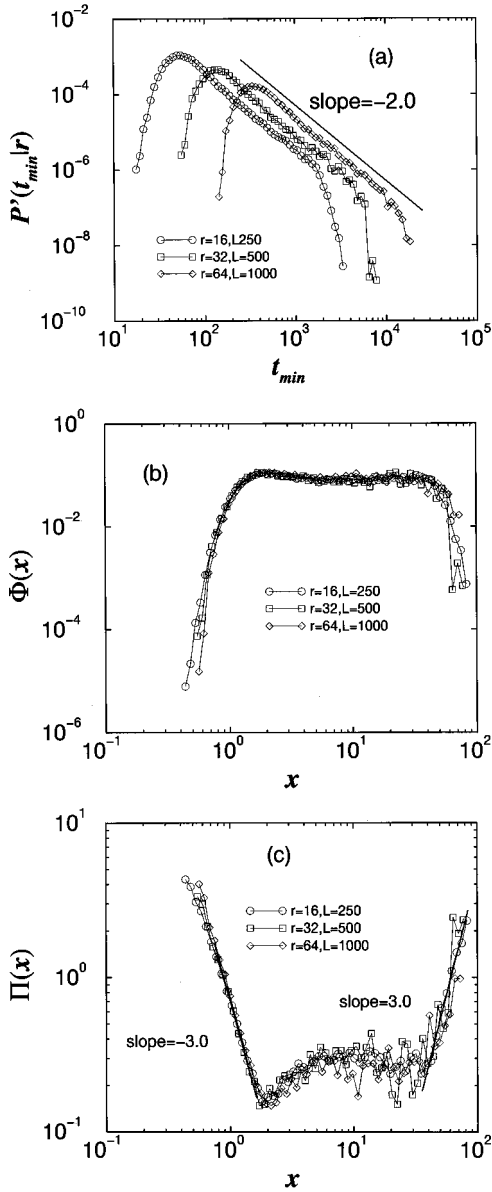


FIG. 5. For $d=2$, (a) log-log plot of $P'(t_{\min}|r)$ for $p=p_c=0.5$ and for different sets of parameters $(r,L)=(16,250)$, $(32,500)$, $(64,1000)$. The straight line regime has slope $g'_t=2.0$. (b) Log-log plot of rescaled probability $\Phi(x)\equiv P'(t_{\min}|r)x^{g'_t}r^{d_{\text{tm}}}$ against rescaled length $x=t_{\min}/r^{d_{\text{tm}}}$ using the values $g'_t=2.0$ and $d_t=1.33$. The curves are flat in the center because $f_2(x)$ is a stretched exponential [see Eq. (25)]. (c) Log-log plot of transformed probability $\Pi(x)=\log_{10}[A/\Phi(x)]$ versus $x=t_{\min}/r^{d_{\text{tm}}}$. The slopes of the solid lines give the power of the stretched exponential function f_1 and f_2 in Eq. (25). Using the parameter $A=0.14$, the slopes give $\phi\approx 3.0$ for the lower cutoff and $\psi\approx 3.0$ for the upper cutoff.

To determine the functions f_1 and f_2 , we compute the rescaled probability distribution

$$\Phi\left(\frac{t_{\min}}{r^{d_{\text{tm}}}}\right)\equiv P'(t_{\min}|r)(t_{\min})^{g'_t}r^{-d_{\text{tm}}(g_{\text{tm}}-1)}, \quad (42)$$

and plot it against the scaling variable $x=t_{\min}/r^{d_{\text{tm}}}$ [see Fig. 5(b)]. According to Eq. (40)

$$\Phi(x)=Af_1(x)f_2\left[x\left(\frac{r}{L}\right)^{d_{\text{tm}}}\right]. \quad (43)$$

Therefore, $\Phi(x)$ should depend only on x and the ratio r/L . Unlike the fractal dimension of the shortest path, d_{\min} , there have been no calculations of the fractal dimension of the minimal traveling time, d_{tm} . We estimate d_{tm} by finding the value that yields the best data collapse for Eq. (43). For $d_{\text{tm}}=1.33$, Fig. 5(b) shows data collapse with sharp cutoffs governed for small $x<1$ by $f_1(x)$ and for large $x>(L/r)^{d_{\text{tm}}}$ by $f_2[x(r/L)^{d_{\text{tm}}}]$.

In order to test the assumption that the functions f_1 and f_2 are stretched exponentials with exponents ϕ_{tm} and ψ_{tm} , we make a log-log plot of $\Pi(x)\equiv\log_{10}[A/\Phi(x)]$ versus x for various values of the normalization constant A [see Fig. 5(c)]. If the stretched exponential conjecture is correct, $\Pi(x)$ should have two straight line asymptotes for $\log_{10}x\rightarrow+\infty$ with the slope ψ_{tm} and for $\log_{10}x\rightarrow-\infty$ with the slope $-\phi_{\text{tm}}$. The slopes ϕ_{tm} and ψ_{tm} of the straight line fits depend weakly on the value of A . Using $A=0.14$, we obtain the longest regimes of straight line behavior. For this A we obtain $\phi_{\text{tm}}\approx 3.0$ and $\psi_{\text{tm}}\approx 3.0$. With the same assumptions we derive Eq. (14), we can derive a similar expression for ϕ_{tm} ,

$$\phi_{\text{tm}}=\frac{1}{d_{\text{tm}}-1}, \quad (44)$$

which yields a predicted value of ϕ_{tm} of 3.0 in agreement with our simulation result.

2. Off-critical behavior

Finally, in order to test the dependence of $P'(t_{\min}|r)$ on p we obtain data for a large system size L ($L=1000$, $d=2$) and for several values of $p\neq p_c$. As we do for the shortest length, we analyze the behavior of t_{\min} in three regimes determined by the relation of the value of the connectedness length ξ to the values of r and L .

(i) $\xi>L>r$. In this regime, the fact that $p\neq p_c$ cannot be detected because the connectedness length is larger than the other relevant variables.

(ii) $L>\xi>r$. In this case, the upper cutoff of the distribution Eq. (38) is governed by f_3 and the functional form of the rescaled probability Φ is given by

$$\Phi\left(\frac{t_{\min}}{r^{d_{\text{tm}}}}\right)\sim f_1\left(\frac{t_{\min}}{r^{d_{\text{tm}}}}\right)f_3\left(\frac{t_{\min}}{\xi^{d_{\text{tm}}}}\right). \quad (45)$$

For large t_{\min} , we suggest an exponential decay [27] of Φ

$$\Phi\left(\frac{t_{\min}}{r^{d_{\text{tm}}}}\right)\sim\exp\left(-c\frac{t_{\min}}{\xi^{d_{\text{tm}}}}\right). \quad (46)$$

Semilogarithmic plots of $\Phi(t_{\min}/r^{d_{\text{tm}}})$ versus t_{\min} for $p>p_c$ and $p<p_c$ shown in Fig. 6(a) and 6(b), respectively, can be approximated by straight lines with slopes that approach zero as $p\rightarrow p_c$. According to Eq. (46), this slope $k(p)$ should follow

$$k(p)\sim\xi^{-d_{\text{tm}}}=|p-p_c|^{d_{\text{tm}}}\approx|p-p_c|^{1.77}. \quad (47)$$

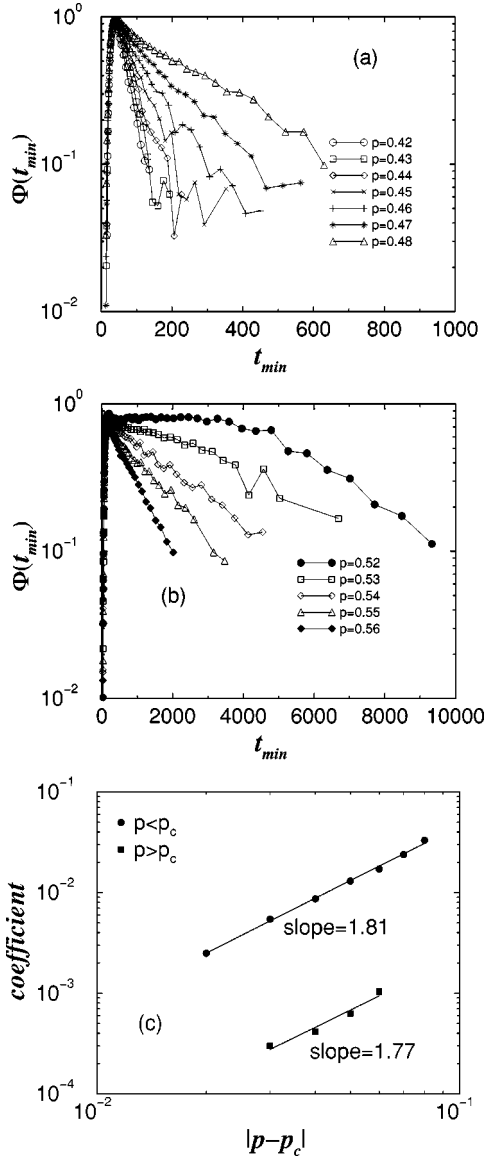


FIG. 6. For $d=2$, (a) semilogarithmic plot of transformed probability $\Phi(t_{\min}/r^{d_{\text{tm}}})$ versus t_{\min} for f_3 for $p=0.42,0.43,0.44,0.45,0.46,0.47,0.48$ below criticality. (b) Same for $p=0.52,0.53,0.54,0.55,0.56$ above criticality. (c) The slope of the log-log plot of the coefficient in the exponential function f_3 as a function of $|p-p_c|$ gives the value $vd_{\text{tm}} \approx 1.77$ for $p > p_c$ and 1.81 for $p < p_c$.

Figure 6(c) shows double logarithmic plots of $|k(p)|$ versus $|p-p_c|$ for $p < p_c$ and $p > p_c$, which can be well approximated by straight lines with slopes 1.81 and 1.77, respectively, in good agreement with the scaling conjecture, Eq. (47). As was the case with the analysis of $P'(\mathcal{L}|r)$ for $p > p_c$ for $d=3$ [see Sec. II D 2, point (ii)], we cannot determine the parameters that govern the large t_{\min} behavior of $P'(t_{\min})$ because of limitations on the size of the system we can simulate.

(iii) $L > r > \xi$. When the connectedness length is smaller than the distance between the wells, the behavior of the system is the same as a homogeneous system [1,3,5]. This can be seen in Fig. 7(a) in which we plot $P(t_{\min}|r)$ for various values of r at $p=0.6$ ($d=2$). As r increases from below to above the connectedness length, the form of the distribution

changes from the power law distribution of Eq. (40) to a distribution with a pronounced peak, a characteristic of homogeneous systems. In Fig. 7(b), in order to eliminate the finite size effect, we select $L=r+2$ so that the distribution $P(t|r)$ does not have a power law regime, even for small r . In this case, as shown in Fig. 7(c), the fractal dimension of the minimal traveling time crosses over from $d_{\text{tm}}=1.33$ to $d_{\text{tm}}=2.0$, characteristic of a homogeneous system [28,29]. The same considerations that we use to derive the behavior of the mean and variance of the shortest path can be applied to the mean and variance of the minimal time. At the moment of breakthrough, i.e., when the first tracer particle reaches the second well, the part of the system filled with tracer particles consists of $n_b=(r/\xi)^d$ independent blobs, each having a certain number of bonds $(t_{\min})_b$ with an average $\langle (t_{\min})_b \rangle = \xi^{d_{\text{tm}}}$ and a variance $\sigma_b^2 = \xi^{2d_{\text{tm}}}$. Thus the average minimal time for the entire system scales as

$$\langle t_{\min} \rangle = n_b \xi^{d_{\text{tm}}} = r^d \xi^{d_{\text{tm}}-d}, \quad (48)$$

with a variance

$$\sigma^2 = n_b \xi^{2d_{\text{tm}}} = r^d \xi^{2d_{\text{tm}}-d}. \quad (49)$$

The scaling plot [Fig. 7(d)] of $\langle t_{\min} \rangle$ versus $|p-p_c|$ shows good agreement with the theoretical prediction of Eq. (48),

$$\frac{\langle t_{\min} \rangle}{r^d} = (p-p_c)^{(d-d_{\text{tm}})\nu} = (p-p_c)^{0.89} \quad (d=2). \quad (50)$$

The graph of σ versus r [see Fig. 7(e)] shows linear behavior, in agreement with Eq. (49). Equation (49) also predicts that the slope of this linear dependence decays as

$$|p-p_c|^{-[d_{\text{tm}}-(d/2)]\nu} = |p-p_c|^{-0.42} \quad (d=2). \quad (51)$$

However, the measured slope has a very small variation with $|p-p_c|$ that is beyond the accuracy of our data points.

As mentioned above, the minimal traveling time is the sum of the inverse local velocities over the fastest path where the fastest path is statistically identical to the shortest path. While the velocity distribution has been studied extensively (see, e.g., [38,39]), because the velocities along the path are correlated, the relation between the minimum traveling time distribution and the local velocity distribution is an open challenge for further research.

The analysis for three dimensions is completely analogous to that for two dimensions. Our results are shown in Figs. 8 and 9 and the scaling parameters found are included in Table I.

Note that the exponent d_{tm} is the fractal dimension of the set of bonds reached by the tracer particles at the moment of breakthrough. A similar problem was studied in [17], where it was found that, when the invading fluid has a lower viscosity than the defending fluid, the fractal dimension of the cluster occupied by the invading fluid at the moment of breakthrough (in $d=2$) is approximately 1.3. This case is analogous to diffusion-limited aggregation in a percolation cluster.

Our case of passive tracer particles corresponds to the equal viscosity of invading and defending fluids. The fact that both exponents in two dimensions are close to each

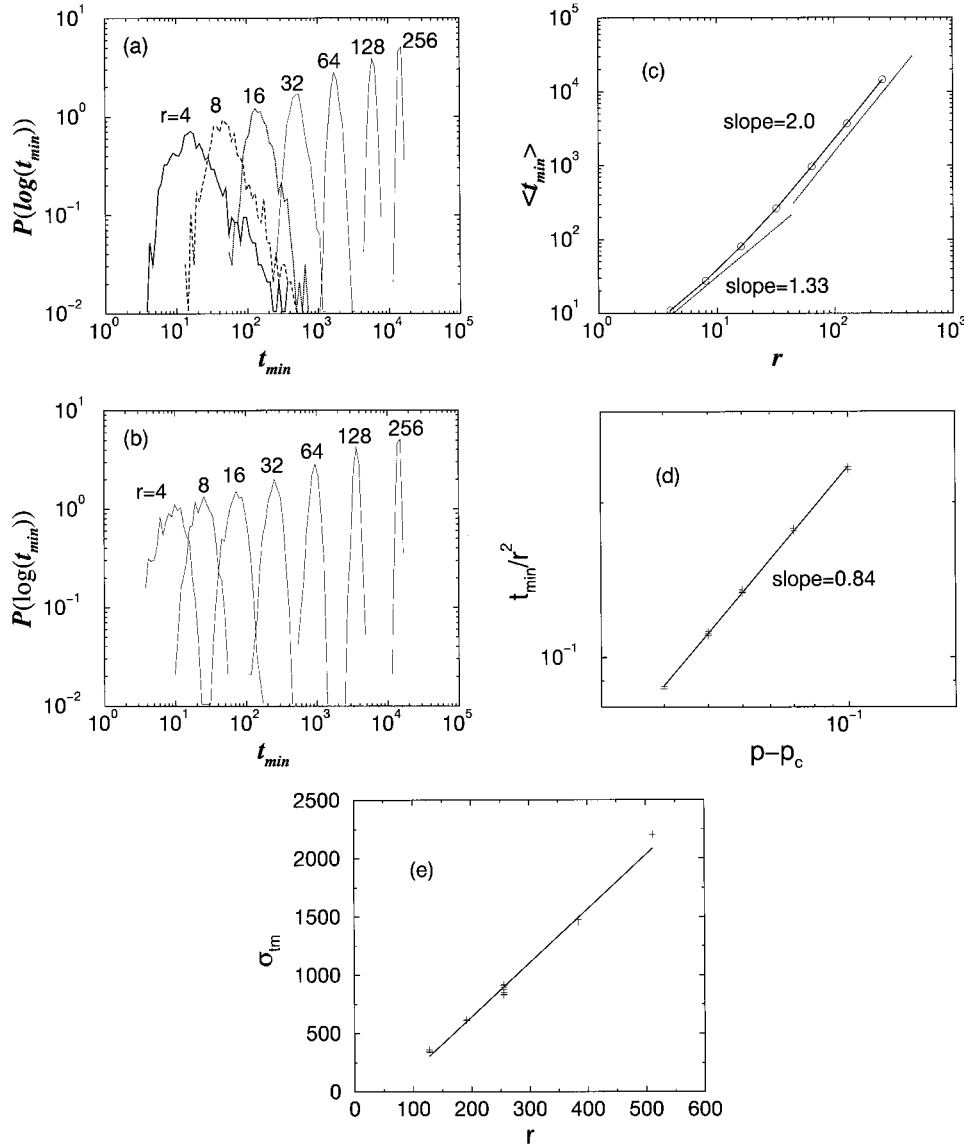


FIG. 7. (a) Log-log plot of $P(t_{\min}|r)$ for $p=0.6$ and for $r=4, 8, 16, 32, 64, 128, 256$ and $L=258$. The distributions for large r converge to Gaussians with mean $\langle t_{\min} \rangle$ and variance σ^2 . (b) Log-log plot of $P(t_{\min}|r)$ for $p=0.6$, $r=4, 8, 16, 32, 64, 128, 256$ and $L=r+2$. [Note that, for this case, where $r > \xi$, the distributions $P'(t_{\min}|r)$ and $P(t_{\min}|r)$ are essentially the same since all the clusters span the lattice.] (c) Log-log plots of $\langle t_{\min} \rangle$ versus r for $p=0.6$ and $L=r+2$. (d) Log-log plot of the scaled average minimal traveling time $\langle t_{\min} \rangle/r^2$ versus $p-p_c$ for $r=128, 192, 256, 384, 512$ and $L=r+2$. Note that in all cases $r \gg \xi$. The slope of the line, 0.84, is in good agreement with the theoretical prediction 0.89. (e) The behavior of the width σ of the distributions of the traveling time versus r for $p=0.53, 0.54, 0.55, 0.57, 0.6$. The graph shows approximately linear dependence of σ on r . The variation of the slope with $p-p_c$ is within the error bars of the data.

other suggests that both cases belong to the same universality class. Our preliminary analysis of DLA in three-dimensional percolation clusters suggests that its fractal dimension is 1.41 ± 0.05 , in good agreement with our result $d_{tm} = 1.45$.

C. Fastest path

We observe that the path which takes minimal time is not always the shortest path. However, analysis of the distributions of ℓ_{\min} yields parameters identical to those for the distribution of the shortest paths between points separated by distance r studied in detail in Ref. [14]. Thus, statistically, the path that takes the shortest time is one of the paths of shortest length.

In many transport problems, the characteristic time t^* scales with the characteristic length ℓ^* with a power law,

$$t^* \sim (\ell^*)^z. \quad (52)$$

Since t^* scales as r^{d_t} and ℓ^* scales as $r^{d_{\min}}$,

$$z = \frac{d_t}{d_{\min}}. \quad (53)$$

Since t_{\min} and ℓ_{\min} are strongly correlated, the distributions $P(\ell_{\min})$ and $P(t_{\min})$ satisfy

$$P(\ell_{\min})d\ell_{\min} = P(t_{\min})dt_{\min}. \quad (54)$$

Combining Eqs. (52)–(54) and the equations for the respective distributions, we obtain a scaling relation between exponents,

$$(g_{\ell_{\min}} - 1)d_{\ell_{\min}} = (g_{t_{\min}} - 1)d_{t_{\min}}. \quad (55)$$

These scaling relations are well satisfied by the set of scaling exponents given in Table I.

D. Dependence of minimal traveling time on resistance

The overall hydraulic resistance R of a percolating system between two sites A and B with pressure difference $P_A - P_B$ is defined as

$$R = \frac{P_A - P_B}{J}, \quad (56)$$

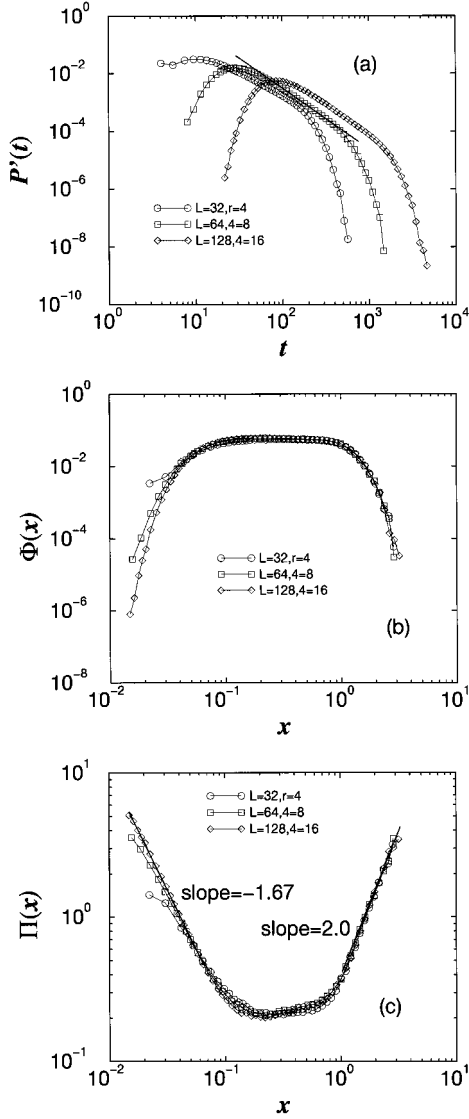


FIG. 8. For $d=3$, (a) log-log plot of $P'(t|r)$ for $p=p_c=0.2488$ and for different sets of parameters $(r,L)=(4,32)$, $(8,64)$, $(16,128)$. The power law regime has slope $g'_t=2.1$. (b) Log-log plot of rescaled probability $\Phi(x)\equiv P'(t_{\min}|r)x^{g'_t}r^{d_{\text{tm}}}$ against rescaled length $x=t_{\min}/r^{d_{\text{tm}}}$ using the values $g'_t=2.1$ and $d_t=1.45$. The curves are flat in the center because $f_2(x)$ is a stretched exponential [see Eq. (25)]. (c) Log-log plot of transformed probability $\Pi(x)=\log_{10}[A/\Phi(x)]$ versus $x=t_{\min}/r^{d_{\text{tm}}}$. The slopes of the solid lines give the power of the stretched exponential functions f_1 and f_2 in Eq. (25). Using the parameter $A=0.08$, the slopes give $\phi\approx 1.6$ for the lower cutoff and $\psi\approx 2.0$ for the upper cutoff.

where J is the total flow defined as the sum of all the velocities outgoing from site A , which is equal to the sum of velocities coming into site B ,

$$J = \sum_i v_{iA} = \sum_i v_{iB}. \quad (57)$$

It is known [1,3] that the typical resistance R^* scales with the distance between sites A and B as

$$R^* \sim r^\mu, \quad (58)$$

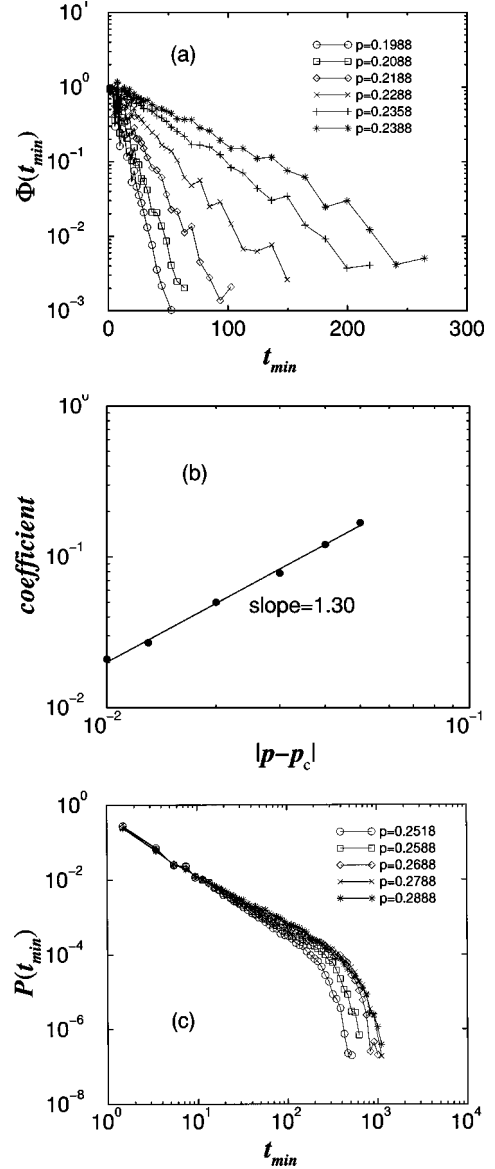


FIG. 9. For $d=3$, (a) semilogarithmic plot of transformed probability $\Phi(t_{\min})$ versus t_{\min} below critical point for $p=0.1988, 0.2088, 0.2188, 0.2288, 0.2358, 0.2388$ shows pure exponential behavior of f_3 . (b) The slope of the log-log plot of the coefficient in exponential function f_3 as a function of $|p-p_c|$ gives the value $\nu d_{\text{tm}}\approx 1.30$ for $p < p_c$. (c) $P(t_{\min})$ for $p > p_c$. Note that for the values of p simulated, the large t_{\min} behavior is determined by the finite size of the system—not f_3 .

where $\mu=0.98$ [35].

We find numerically that resistance strongly correlates with both minimal traveling length [36]

$$\ell_{\min} \sim R^{d_{\text{tm}}/\mu} \quad (59)$$

and minimal traveling time

$$t_{\min} \sim R^{d_{\text{tm}}/\mu}. \quad (60)$$

Accordingly, the distribution of the resistance should obey the same scaling ansatz as Eqs. (18) and (38),

TABLE I. Summary of exponents and coefficients in scaling form $P(x|r) \sim (1/r^{d_x})(x/r^{d_x})^{-g_x} f_1(x/r^{d_x}) f_2(x/L^{d_x}) f_3(x/\xi^{d_x})$, where $f_1(y) = \exp(-a_x y^{-\phi_x})$, $f_2(y) = \exp(-b_x y^{\psi_x})$, $f_3(y) = \exp(-c_x y)$. Here x denotes one of the quantities ℓ or t_{\min} . The notation N/A means not applicable (since no theoretical value exists), while the notation (+/-) indicates above or below p_c .

x exponent	ℓ		t_{\min}	
	Simulation	Theory	Simulation	Theory
		$d=2$		
d_x	1.13 ± 0.01	N/A	1.33 ± 0.05	N/A
g'_x	2.14 ± 0.02	2.11	2.0 ± 0.1	N/A
a_x	0.5	N/A	1.1	N/A
ϕ_x	7.3 ± 0.5	$1/(d_x - 1) = 7.69$	3.0	3.0
b_x	3.5	N/A	5.0	N/A
ψ_x	4.0 ± 0.5	N/A	3.0	N/A
c_x	$2.4(-), 3.7(+)$	N/A	$1.6(-), 2.6(+)$	N/A
		$d=3$		
d_x	1.39 ± 0.05	N/A	1.45 ± 0.10	N/A
g'_x	2.3 ± 0.1	2.23	2.1 ± 0.1	N/A
a_x	1.4	N/A	2.5	N/A
ϕ_x	2.1 ± 0.5	$1/(d_x - 1) = 2.56$	1.6	2.0
b_x	2.0	N/A	2.3	N/A
ψ_x	2.5 ± 0.5	N/A	2.0	N/A
c_x	$3.1(-)$	N/A	$2.9(-)$	N/A

$$P'(R|r) \sim \frac{1}{r^\mu} \left(\frac{R}{r^\mu} \right)^{-g'_R} f_1 \left(\frac{R}{r^\mu} \right) f_2 \left(\frac{R}{L^\mu} \right) f_3 \left(\frac{R}{\xi^\mu} \right), \quad (61)$$

with the exponent μ playing the role of the resistance fractal dimension and the exponent $g'_R \approx 2.3$ obeying the relation

$$\mu(g'_R - 1) = d_{\min}(g'_\ell - 1). \quad (62)$$

We tested the scaling ansatz (61) numerically and found agreement with our theoretical predictions.

In industrial applications, it is very important to predict the time of the breakthrough of the injected fluids into the production well [28]. Since the pressure and the flow are known immediately as the operation of the well begins, one can predict t_{\min} using the relationship (60).

Up to now, we have considered the breakthrough time distribution for the case of a fixed injection rate $J = \text{const}$. Another practical application is related to the distribution of breakthrough time at a constant pressure difference $P_A - P_B = \text{const}$. For each configuration of the porous medium with resistance R , the minimal traveling time at constant pressure, \hat{t}_{\min} , is related to the minimal traveling time t_{\min} at constant flow as

$$\hat{t}_{\min} = R t_{\min}. \quad (63)$$

Using Eqs. (60) and (63) we conclude that the distribution of \hat{t}_{\min} should obey the same scaling ansatz (38) in which t_{\min} is replaced by \hat{t}_{\min} and exponents d_{tm} and g'_{tm} are replaced by exponents $d_{\text{tmp}} = d_{\text{tm}} + \mu \approx 2.3$ and $g'_{\text{tmp}} = (g'_{\text{tm}} - 1)(d_{\text{tm}}/d_{\text{tmp}}) + 1 \approx 1.57$, respectively. We tested the scaling ansatz (38) for \hat{t}_{\min} numerically and found agreement between the numerically determined values of d_{tmp} and g'_{tmp} and our theoretical predictions.

IV. CONCLUSIONS

By modeling porous media using bond percolation and concepts of percolation theory, we study the flow of fluid in porous media in two and three dimensions between two ‘‘wells’’ separated by Euclidean distance r . We investigate the distribution function of the shortest path connecting the two sites, and propose a scaling ansatz that accounts for the dependence of this distribution (i) on L , the size of the system, and (ii) on p , the bond occupancy probability. We confirm by extensive simulations that the ansatz holds for $d = 2, 3$, and we calculate the relevant scaling parameters.

In order to understand the properties of the flow of oil displaced by fluid or gas, we study the dynamics of flow on percolation clusters. We study two dynamical quantities: the minimal traveling time and the length of the path corresponding to the minimal traveling time. Because of the approximate parallel between the shortest path and the minimal traveling time of flow, the study of the *shortest* path is the first step in understanding the properties of oil fields. In particular, a scaling ansatz for these dynamical quantities includes the effect of finite system size and off-critical bond occupation probability. We find that the scaling form for the distribution functions for these dynamical quantities for $d = 2, 3$ is similar to, *but not identical to*, that for the shortest path. In addition to calculating the relevant distribution functions and scaling relations, we determine the constants and exponents which characterize these relations (see Table I).

ACKNOWLEDGMENTS

We thank BP Amoco and CNPq for financial support, and M. Barthél my, A. Coniglio, J. Koplik, S. Redner, and R. M. Ziff for helpful discussions.

- [1] D. Stauffer and A. Aharony, *Introduction to Percolation Theory* (Taylor & Francis, Philadelphia, 1994).
- [2] S. Havlin and D. Ben-Avraham, *Adv. Phys.* **36**, 695 (1987).
- [3] *Fractals and Disordered Systems*, edited by A. Bunde and S. Havlin (Springer-Verlag, New York, 1996).
- [4] M. Sahimi, *Rev. Mod. Phys.* **65**, 1393 (1993).
- [5] M. Sahimi, *Applications of Percolation Theory* (Taylor & Francis, London, 1994).
- [6] *The Fractal Approach to Heterogeneous Chemistry: Surfaces, Colloids, Polymers*, edited by D. Avnir (John Wiley & Sons, Chichester, U.K., 1989).
- [7] E.T. Gawlinski and H.E. Stanley, *J. Phys. A* **14**, L291 (1981).
- [8] A. Geiger and H.E. Stanley, *Phys. Rev. Lett.* **49**, 1895 (1982).
- [9] P.G. de Gennes, *Scaling Concepts in Polymer Physics* (Cornell University Press, Ithaca, NY, 1979).
- [10] J.M. Ziman, *Models of Disorder* (Cambridge University Press, Cambridge, 1979).
- [11] V. Ambegaokar, B.I. Halperin, and J.S. Langer, *Phys. Rev. B* **4**, 2612 (1971).
- [12] A.J. Katz and A.H. Thompson, *Phys. Rev. B* **34**, 8179 (1986); *J. Geophys. Res. B* **92**, 599 (1987).
- [13] J.S. Andrade, Jr., D.A. Street, Y. Shibusa, S. Havlin, and H.E. Stanley, *Phys. Rev. E* **55**, 772 (1997).
- [14] N.V. Dokholyan, Y. Lee, S.V. Buldyrev, S. Havlin, P.R. King, and H.E. Stanley, *J. Stat. Phys.* **93**, 603 (1998); N.V. Dokholyan, S.V. Buldyrev, S. Havlin, P.R. King, Y. Lee, and H.E. Stanley, *Physica A* **266**, 53 (1999).
- [15] Y. Lee, J.S. Andrade, Jr., S.V. Buldyrev, N. Dokholyan, S. Havlin, P.R. King, G. Paul, and H.E. Stanley, *Phys. Rev. E* **60**, 3425 (1999).
- [16] P. R. King, in *North Sea Oil and Gas Reservoirs III*, edited by A. T. Buller *et al.* (Graham and Trotman, London, 1990).
- [17] M. Murat and A. Aharony, *Phys. Rev. Lett.* **57**, 1875 (1986).
- [18] Z. Alexandrowicz, *Phys. Lett.* **80A**, 284 (1980).
- [19] R. Pike and H.E. Stanley, *J. Phys. A* **14**, L169 (1981).
- [20] H.J. Herrmann and H.E. Stanley, *J. Phys. A* **21**, L829 (1988).
- [21] P. Grassberger, *J. Phys. A* **25**, 5475 (1992).
- [22] P. Ray, *J. Phys. A* **18**, L657 (1985).
- [23] M. Barma and P. Ray, *Phys. Rev. B* **34**, 3403 (1986).
- [24] A.U. Neumann and S. Havlin, *J. Stat. Phys.* **52**, 203 (1988).
- [25] R.M. Ziff, *J. Phys. A* **32**, L457 (1999).
- [26] P.L. Leath, *Phys. Rev. B* **14**, 5046 (1976).
- [27] The decay could, of course, be more generally a stretched exponential of the form $\exp(-cx^\varphi)$ but, within the limits of our simulations, we could not distinguish a value of φ close to but not equal to 1 from a value of $\varphi = 1$.
- [28] P. King, J.S. Andrade, Jr., N.V. Dokholyan, S.V. Buldyrev, S. Havlin, Y. Lee, and H.E. Stanley, *Physica A* **266**, 107 (1999).
- [29] J. Koplik, S. Redner, and E.J. Hinch, *Phys. Rev. E* **50**, 4650 (1994).
- [30] P.G. Saffman, *J. Fluid Mech.* **6**, 321 (1959).
- [31] J. Koplik, S. Redner, and D. Wilkinson, *Phys. Rev. A* **37**, 2619 (1988).
- [32] J.-C. Bacri *et al.*, in *Hydrodynamics of Dispersed Media*, edited by J.P. Hulin, A.M. Cazabat, E. Guyon, and F. Carmona (Elsevier/North-Holland, Amsterdam, 1990), p. 249.
- [33] M. Sahimi, *Flow and Transport in Porous Media and Fractured Rock* (VCH, Boston, 1995).
- [34] F.A.L. Dullien, *Porous Media—Fluid Transport and Pore Structure* (Academic Press, New York, 1979).
- [35] P. Grassberger, *Physica A* **262**, 251 (1999).
- [36] G. Paul, S.V. Buldyrev, N.V. Dokholyan, S. Havlin, P.R. King, Y. Lee, and H.E. Stanley, *Phys. Rev. E* **61**, 3435 (2000).
- [37] H.J. Herrmann and H.E. Stanley, *Phys. Rev. Lett.* **53**, 1121 (1984).
- [38] L. de Arcangelis, S. Redner, and A. Coniglio, *Phys. Rev. B* **31**, 4725 (1985).
- [39] M. Barthélémy, S.V. Buldyrev, S. Havlin, and H.E. Stanley, *Phys. Rev. E* **61**, 3283 (2000).